Bachelor Thesis

Pd Plasmonic Nanocapsules: Synthesis, Characterization and Applications

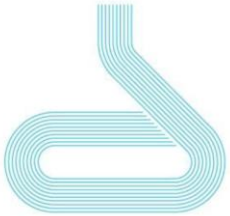

Facultade de Química

Lucía Gil Fandiño

Supervisors: Isabel Pastoriza Santos, Jorge Pérez Juste

ACADEMIC YEAR 2019/20 | BACHELOR IN CHEMISTRY - UNIVERSITY OF VIGO (SPAIN)

Acronyms and Notation

AA: L-Ascorbic Acid

CB: Conduction Band

CTAB: Hexadecyltrimethylammonium Bromide

E_F: Fermi Energy

ε_m: electric permittivity

IR: Infrared Radiation

LSP: Localized Surface Plasmons

LSPR: Localized Surface Plasmons Resonance

NP: nanoparticle

Ox.: oxidation

Red.: reduction

Res.: restorer

rpm: revolution per minute

SERS: Surface-Enhanced Raman Scattering

TEM: Transmission Electron Microscopy

UV-vis: Ultraviolet-visible

VB: valence band

λ: wavelength

$\sigma_{ext.}$: extinction cross-sections

Φ_B: height of the Schottky barrier

Contents

1. Abstract

Nanotechnology is developed through handling of materials at nanometric scale. Some nanomaterials show properties that are unique to their scale. This is the case of Pd, an element that has an extraordinary catalytic capacity, plus an important thermic stability. In the Pd nanoparticles (NPs), the catalytic capacity could be strengthened thanks to the optical properties that the material acquires at nanometric scale. This study begins with the synthesis of Au nanocapsules, a model system employed to acquire the necessary knowledge (synthesis and characterization methods) for the fabrication of Pd capsules. Later, it would have continued with the synthesis and characterization of Pd nanocapsules, looking for this synergy between the optical and catalytic properties. However, due to the irruption of the COVID-19 pandemic, this synthesis of Pd nanocapsules could not be carried out and the work done in laboratory has been complemented with a bibliographic revision. In this context, the lack of literature about Pd nanocapsules shifted our focus to the synthesis, characterization and photocatalytic applications of nanocapsules made of Ag-Pd alloys. The synthesis of the nanocapsules is carried out in two different ways: via galvanic replacement combined with correduction, and without the combination. Results support correduction as the more robust alternative. In the Ag-Pd nanocapsules, the exceptional optical response of the Ag in the range of the UV-vis and near IR, strengthens the catalytic capacity of the Pd. Also, the high surface/volume ratio of the NPs increases even more the reactive yield of the catalysed reactions, as they are developed on the surface. The extraordinary capacity of the Pd surfaces for the adsorption of H_2 (g) molecules, turns this kind of nanocapsules into outstanding mediators in which multitude of organic reactions that involve proton transfer can be catalysed without the generation of residues toxic to people and environment.

2. Introduction

The colour of a material depends among other things on its response to light. For instance, stained glass like the ones found in Gothic cathedrals, known for their lively colours, are a result of mixing different impurities into the glass during their elaboration [1,2]. Materials can also present different colours when illuminated differently. A notorious example of this is the Lycurgus Cup [2], a 4th Century roman goblet that changes colour depending on the angle of illumination. After numerous attempts to give an answer to this optical phenomena**,** one major advance came about in the middle of the 19th Century, with James Clerk Maxwell's extraordinary work on electromagnetism, which opened the doors to the study and development of many different phenomena in the field of Optics. Maxwell unified in a few equations the behaviour of electric and magnetic fields, which were studied separately until that moment. Extraordinarily, these few equations also explain the materials' quantum response to light, leading to decades of study and investigation in this field as well.

When a material is illuminated, it is being hit by quanta of energy (Photons) that travel like electromagnetic waves. They can be reflected and/or refracted by the material, and it is also known that a certain amount is absorbed and/or scattered. According to the *Law of conservation of energy*, the absorbed and/or scattered radiation is converted in other forms of energy, so the more capacity a material presents, the more energy will be converted. For nanoparticles of a given size, the material's capacity to absorb/scatter incoming electromagnetic radiation is determined by its extinction cross-section ($\sigma_{ext.}$) [2,3]. Expressed as a surface, one would think *a priori* that it is smaller than the particle's exposed surface, since there are some zones where light is reflected and/or refracted, and they are not to be taken into account. But it turns out that the $\sigma_{ext.}$ for Au and Ag nanoparticles (NPs) is notably greater that their border surface [2] [Figure 1A] [4] This makes their optical properties of great interest, since very small sizes particles are capable to transform very big amounts of energy when they are illuminated [2,5]. It was in the early 20th Century when the German physicist Gustav Mie achieved an analytical solution, based in Maxwell's equations, to the absorption and scattering phenomena in diminutive spherical particles ($d << \lambda$) [3] [Figure 1B].

A

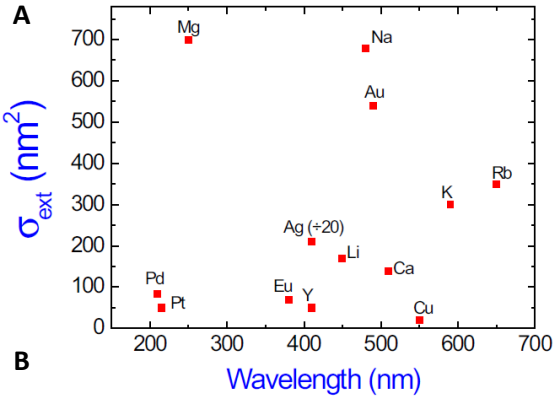

B

$$\sigma_{ext} = \frac{18\,\pi\varepsilon_m^{3/2}V}{\lambda}\,\frac{\varepsilon_2(\lambda)}{[\varepsilon_1(\lambda)+2\varepsilon_m]^2+\varepsilon_2(\lambda)^2}$$

ε_m: función dieléctrica del medio
ε_1 y ε_2: componentes de la función dieléctrica compleja del metal
V: volumen de partícula

Figure 1. (A) extinction cross-sections and resonant frequency in air for various metals (particle size < 10 nm). The $\sigma_{ext.}$ of Ag has been divided by 20 [4]**; (B) Mie equation for the absorption and scattering phenomena in tiny spherical particles [3].

As already mentioned, light arrives to the particle like electromagnetic waves. The wavelengths (λ) for the visible spectrum comprise between 400 and 750 nm. These wavelengths are much bigger than the NPs' radius studied by Mie, so the wave effect on the particle, specifically the electric field effect, is uniform the vast majority of the time [2,6] [Figure 2] [7]. The material's conduction electrons move in the opposite direction to the field lines, thus generating a dipole in the NPs and creating at the same time a new electric field that drags the electrons to their equilibrium position [1] through a force known as restoring force [2] [Figure 2] [7].

The simultaneous oscillation of the conduction electrons is known in this context as plasma. Plasma is quantified by plasmons, and the corresponding oscillation frequency is named plasma frequency [1,2]. Since oscillation occurs near to the interface and the NPs' volumes are very small, these plasmons are specifically called localized surface plasmons (LSPs) [7].

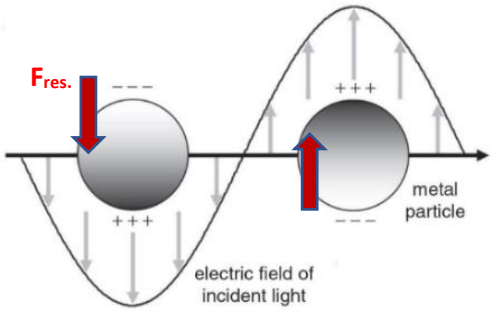

Figure 2. Localized surface plasmons (LSPs). Red arrows indicate the direction of the restoring force [7]*.

When both frequencies (the frequencies of light' electromagnetic waves and the plasma frequencies of NPs) couple, this produces the localized surface plasmons resonance (LSPR) phenomenon [1], by which the amplitude of electron oscillation is maximal. This means that the NP has absorbed the maximum possible energy from the radiation. The imaginary part of the dielectric function of each material makes possible to know the LSPR frequency and therefore the wavelengths of maximum absorption [5] [Figure 3] [5]. The conduction electrons in Au and Ag are far away from the nuclei, practically they are free. This is the reason for the very high $\sigma_{ext.}$ in these nanomaterials [2], since the LSPR occurs in the vicinity of the geometric section of the material.

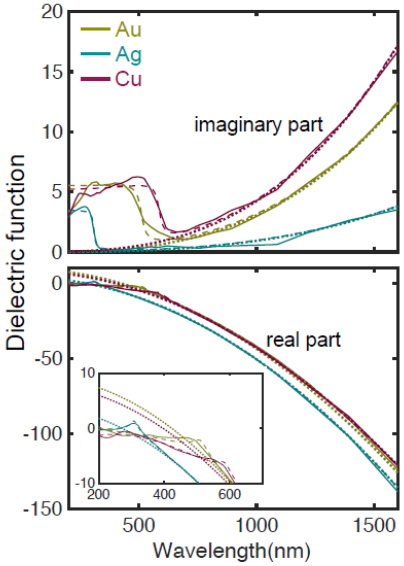

Figure 3. Dielectric functions for three noble metals (particle size < 10 nm) [5]***.

One of the fundamental advantages of working with LSPs is the ability to obtain responses under specific frequencies only. This wouldn't be possible without our ability to manipulate the NP synthesis with regard to shape, size, medium in which they are synthesized, etc [1,2,6,7]. For instance, the bigger the material dimensions are, the higher wavelength the maximum absorption band will have [Figures 4A and 4B] [6]. Regarding shape, there are also several possibilities, e.g. nanorods that feature two different LSPs: one in the vertical section, with a LSPR at lower wavelengths, and other in the base, with a LSPR at higher wavelengths [Figure 4C] [1]. Furthermore, each material (medium) is defined by a specific electric permittivity (ε_m), which describes how polarizable the medium is: for a higher permittivity, the dipole moment in the NPs more decreases, displacing the LSPR band to higher wavelengths [Figure 4D] [3]. Finally, it is fundamental to take into account the interactions between NPs themselves; the interelectronic interactions that occur have a dampening effect upon the LSPs, displacing the LSPR band to higher wavelengths [Figure 4E] [8].

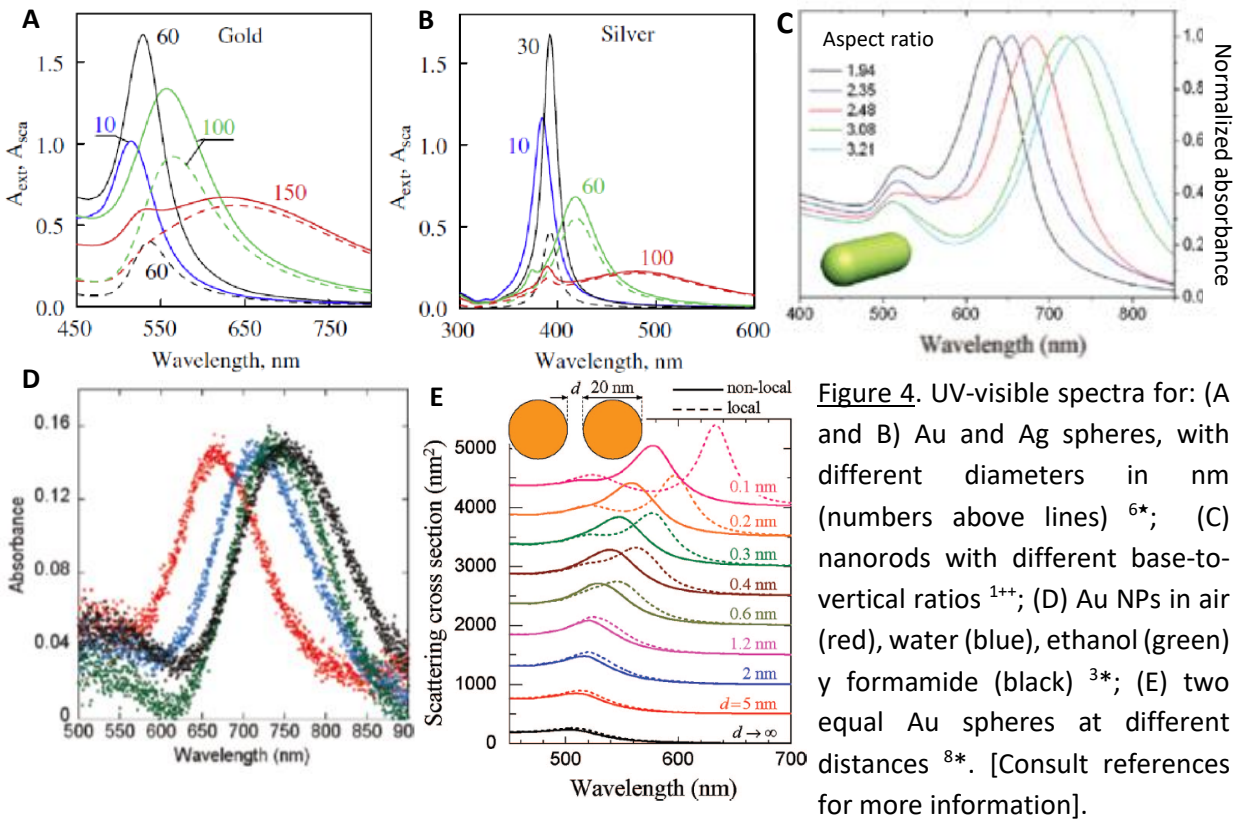

Figure 4. UV-visible spectra for: (A and B) Au and Ag spheres, with different diameters in nm (numbers above lines) [6]*; (C) nanorods with different base-to-vertical ratios [1++]; (D) Au NPs in air (red), water (blue), ethanol (green) y formamide (black) [3]*; (E) two equal Au spheres at different distances [8]*. [Consult references for more information].

Through a technique known as galvanic replacement [9–13], it is possible to induce the formation of cavities inside of the NPs. It is developed based on REDOX reactions, in which the outer metal of the NPs is oxidized, and simultaneously a second metal is reduced and deposits on the NPs surface. Thus, as the reactions progresses, a hollow capsule is conformed due to the emptying of material that at first established the outer part of the NPs [Figure 5] [11]. This process can be enhanced via correduction by adding a mild reducing agent, which confers control over the reacting course, and also alters the way in which NP surfaces corrode. Another way to enhance the galvanic replacement process is by working with NPs which contain an interior nucleus. Both improvements contribute to morphological consistency, since they enable us to control that an excessive transmetalation leading to NP fragmentation does not occur [12].

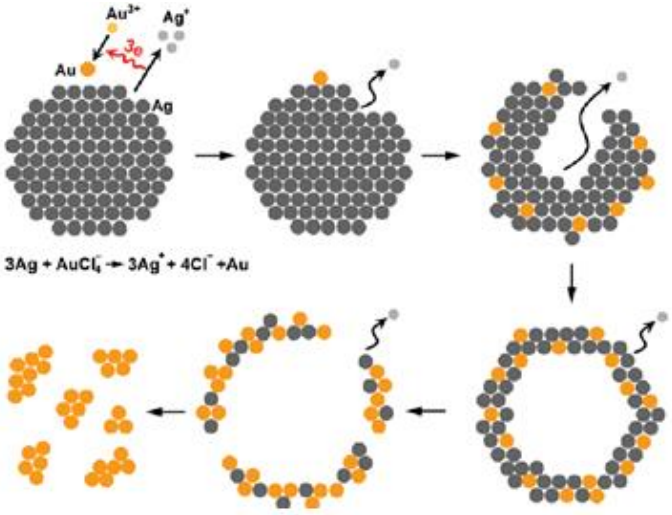

Figure 5. Outline of the galvanic replacement process for the formation of Ag-Au nanocapsules followed by an excessive transmetalation that results in fragmentation [11]**.

In the vast majority of cases, the NPs LSPR manifests at lower frequencies than the LSPRs of precursor compact NPs [Figure 6] [10], as a result of coupling the outer and inner LSPs. Prodan et al. explain this phenomenon according to a hybridization model, in which more complex geometries are decomposed in simpler geometries. They propose a "hybridization" between the LSPs of spherical NPs and the LSPs of nanocavities in bulk metals [Figure 7] [14]. In the resulting nanocapsules, both LSPs are separated by a thin layer only (the capsule), so that an interaction among them is produced.

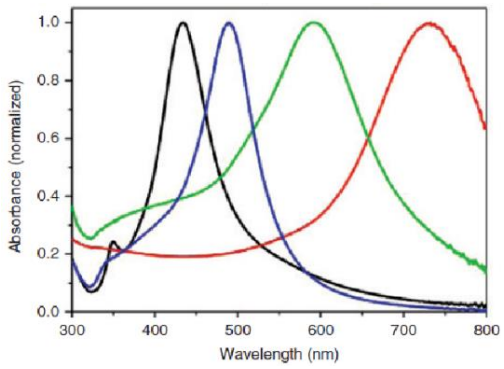

Figure 6. UV-visible spectra of Ag nanocubes (black), Ag@Au core-shell nanocubes (blue), Au-Ag pinholed nanoboxes (green) and Au-Ag single-walled nanoboxes (red) [10++].

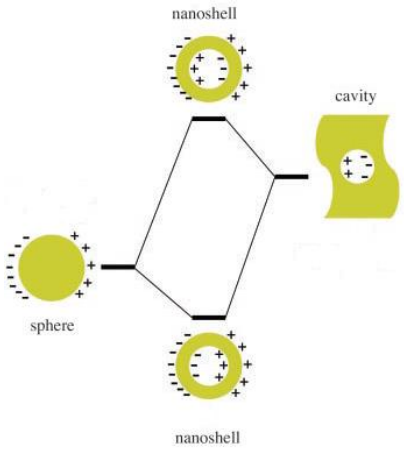

Figure 7. Energy-level diagram for the nanocapsule formation as given by the hybridization model of the LSPs [14+].

Again, the scientist has the capability to handle those interactions, by modifying the shell thickness. The thinner it is, the lower frequency will LSPR occur at, since the outer and inner coupling is higher. The mechanism that provides this capability to vary the shell thickness, allowing to increase it, is named template regeneration [13] [Figure 8] [13]. Due to the existence of pores in the nanocapsules, like the Ag-Pd studied, and the fact that the diffusion rate of the atoms through the alloy matrix is higher than the deposition rate, it is possible to fill the inner hollow with the metal that formed part of the precursor compact NPs. In function of the degree of filling, it becomes possible to control the corresponding degree of growth of the shell though galvanic replacement.

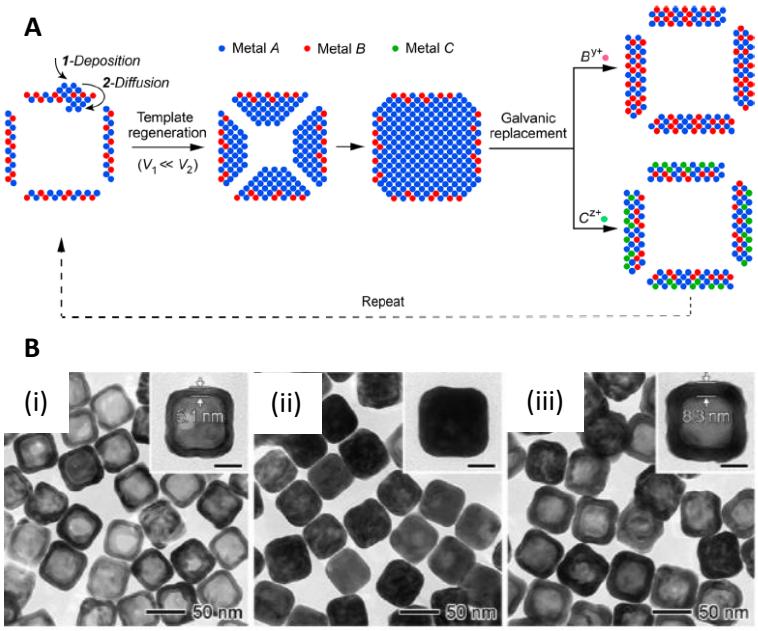

Figure 8. *Template regeneration*: (A) outlined mechanism [13]*; (B) TEM images of (i) Ag-Pd nanoboxes, (ii) Ag@Ag-Pd nanocubes and (iii) Ag-Pd nanoboxes [13]*.

The amplitude in plasmonic response of metals like Au and Ag when visible and near-IR light incides over them, allows us to utilize these materials to enhance or design techniques that use non-invasive and highly available radiation while having high specificity and sensitivity.

Also, to ensure the applicability, the exterior surface of the NPs must be covered with molecules that provide them with coloidal stability. This process is known as functionalization [15], and can also play a key role in the application itself. For example, therapeutic applications like drug delivery and the photothermal treatment [1,2,7] of carcinogenic cells: the NPs can be functionalized with certain molecules that specifically anchor to others present in target cells. Then, when applying IR radiation, the high amplitude of the resulting plasmonic resonance translates into high temperatures, that can break down the molecular cover of the NPs' functionalization, thus allowing the drug delivery through the pores, or even producing the cellular lysis (carcinogenic cells).

Various studies make a comparison in terms of effectiveness of using nanocapsules versus using compact NPs. Gao et al. studied plasmonic responses of both NPs types, using them as colorimetric tags in biosensors [1,7,10,13]. The detection sensitivity achieved using nanocapsules was notably higher than using compact NPs, reporting detection limits up to ten times lower using the nanocapsules and higher colour intensities in the test lines. Schwartzberg et al. analysed the plasmonic response to light scattering on an analyte for an equal amount of nanocapsules and compact NPs, by means of SERS [1,7,10,16]. Results leave no room for doubt of the enormous efficacy of using nanocapsules for this application, since they not only obtained a clearly more intense response, but also the frequencies distribution on the results was narrower.

Finally, and focusing our attention on the use of Ag-Pd nanocapsules, the *par excellence* application is the photocatalysis [10,11,17,18]. The contact between a material with extraordinary optical properties, with a conductor or semiconductor material, promotes a decrease of the prohibited interval in the latter. Besides, when the structure is illuminated and the LSPRs are produced, conduction electrons from the plasmonic material can jump to the conduction band of the conductor or semiconductor material [figure 9] [18]. Both consequences of this alloy enhance the catalytic capacity of the ensemble, just by simply radiating it with visible light. Hydrogenation and dehydrogenation reactions are commonly catalysed with Pd because of its high H_2 (g) adsorption capacity on its surface.

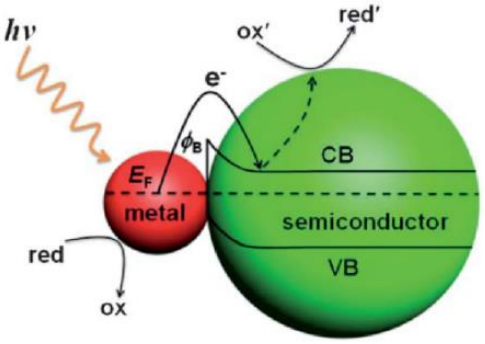

Figure 9. Schema of the photocatalysis process between a metal with plasmonic properties and a semiconductor. CB = conduction band; VB = valence band; E_F = Fermi energy; Φ_B = height of the Schottky barrier [18***].

3. Objectives and work plan

Initially, the purpose of this work was the synthesis and characterization of Pd nanocapsules, as well as the study of their photocatalytic properties. For that, the sub-objectives listed in [Table 1] were outlined. Due to the present situation induced by the COVID-19 pandemic, not all sub-objectives could be reached, due to access restrictions to the University dependencies. In those cases, we resorted to a bibliographic revision.

Table 1. Sub-objetives for the study of synthesis, characterization and application of Pd nanocapsules. It is specified if they were carried out experimentally in the laboratory (exp) or through bibliographic analysis (bibl).

Sub-objectives	Development
1) Formation and characterization of Au@Ag core-shell NPs 2) Formation and characterization of Au nanocapsules.	Exp.
3) Formation and characterization of Pd nanocapsules. 4) Analysis of catalytic capacities of Pd nanocapsules.	Bibl.

Sub-objectives 1) and 2) were the only ones that could be carried out experimentally. Their goal is to get acquainted with the techniques involved, interpretation of spectra, etc. The formation of Au nanocapsules is performed via galvanic replacement, combined with correduction using a mild reducing agent. The planned characterization techniques included UV-visible spectroscopy, TEM and DLS, but only UV-vis spectroscopy could be carried out before the COVID-19 outbreak.
Sub-objectives 3) and 4) aim to synthesize, characterize and study the photocatalytic properties of Pd nanocapsules. Given the fact that they had to be carried out bibliographically, and that current research literature on the topic is very scarce, the focus switched to synthesis, characterization and photocatalytic properties of Pd alloyed with Ag and/or Au. The formation of such nanocapsules is carried out in two different ways: via galvanic replacement combined with correduction using a mild reducing agent, and galvanic replacement without combining with correduction.

4. Experimental procedure

· **Materials:** hexadecyltrimethylammonium bromide (CTAB; $CH_3(CH_2)_{15}N(Br)(CH_3)_3$) ≥96%, Sigma Aldrich; iron sulphate heptahydrate ($FeSO_4 \cdot 7H_2O$) ≥99%, Sigma Aldrich; L-Ascorbic acid (AA) ≥99%, Sigma Aldrich; silver nitrate ($AgNO_3$) ≥99%, Sigma Aldrich; sulfuric acid (H_2SO_4) 95%-97%, Scharlau; tetrachloroauric (III) acid trihydrate ($HAuCl_4 \cdot 3H_2O$) 99.99%, Alfa Aesar; trisodium citrate dihydrate (trisodium citrate; $Na_3C_6H_5O_7 \cdot 2H_2O$) ≥98%, Sigma Aldrich.
Ultrapure water is used for all procedures (18.2 MΩ·cm at 25°C).

· **NPs synthesis:** 150 mL of a $HAuCl_4 \cdot 3H_2O$ 0,5 mM solution are prepared. Then, the solution is placed in the fume Hood with constant stirring and boiling temperature, maintaining reflux

throughout the whole process. Also, 7.5 mL of a trisodium citrate 1% (m/v) solution are also prepared, and situated "near" the hot plate so that when it is added to the Au (III) solution, the temperature change is not so abrupt. At the time that the Au (III) solution begins to boil, the trisodium citrate solution is quickly added, and then we wait for about 15 minutes. Then, the solution is let cooling down until it reaches ambient temperature.

For the particle growths, two solutions are prepared and simultaneously injected on a third solution which has Au seeds. The first solution prepared contains 32 mL of $FeSO_4 \cdot 7H_2O$ 4 mM and trisodium citrate 4 mM. The second solution prepared contains 32 mL de $AgNO_3$ 1mM. Both solutions are introduced in syringes and drop by drop injected through a syringe pump (*Standard Infuse/Withdraw PHD 22/2000 Syringe Pumps* model) on the third solution, making sure that the drops out of both syringes do not make contact. The third solution prepared contains 15 mL of Au 0.1 mM and trisodium citrate 2 mM over a pH=4, that is achieved adding 180 µL of H_2SO_4 0.1 M. The addition is carried out at a rate of 30 mL/h in two batches of 15 mL, and at room temperature.

After the first addition, trisodium citrate is added in order to maintain its concentration at approximately 2 mM and getting so a dissolution of Au@Ag NPs (d = 30 nm approx.). Then, 2/3 of the volume are retired, and we proceed to the second addition, of 15 mL also for each syringe. After that, trisodium citrate is again added in order to maintain the concentration at approximately 2 mM, thus obtaining a dissolution of Au@Ag NPs (d = 50 nm approx.) 0.356 mM. Then, in order to eliminate dissolved molecules, the dissolution is washed. For that, fractions of 5 mL are centrifuged at 2500 rpm for 10 minutes. Then, after removing the supernatant, the pellet of particles from each centrifuged fraction are concentrated in 500 µL of trisodium citrate 1 mM. Finally, all fractions are mixed, obtaining a solution of Au@Ag NPs (d = 50 nm approx.) 3.56 mM.

The Au@Ag NPs (d = 50 nm approx.) are functionalized with CTAB. For it, 1 mL of a dilution 1.60 mM, obtained from the NP solution, is added onto 4 mL of a CTAB 100 mM solution. Then, 0.1 mL of AA 200 mM are further added. From that moment, it begins the continuous, regular and drop by drop addition of 4 mL of a $HAuCl_4 \cdot 3H_2O$ 0,5 mM solution, using the syringe pump programmed to a rate of 50 µL/min.

· **Characterization techniques:** UV-visible spectrophotometry and TEM. The characterization through UV-vis. spectrophotometry is implemented in a spectrophotometer, model *Agilent 8453*. Using this technique, the interaction between the electromagnetic waves of the UV, visible and near IR zones and the NPs can be studied. The absorbed and scattered radiation produces electronic excitations in the NPs, excitations that can be quantified based on the resultant vibrational frequencies. The characterization through TEM allows to study the NPs morphology in function of the scattering degree of the electrons from an accelerated beam that goes through the sample. Gray-contrast images are obtained in function of the thickness of the traversed sections [19]. The characterization through DLS allows to study the diffusion of the NPs across the solution where they are, thus obtaining values as the hydrodynamic radio and their Z potential [20].

5. Presentation and discussion of results

5.1. Formation and characterization of Au@Ag core-shell NPs

Au@Ag core-shell NPs of ca. 50 nm diameter were synthesized for their subsequent use as templates for the capsule formation. First, smaller Au spherical NPs of 14 nm of diameter approx. were synthesized (seeds), via *Turkevich* method [21,22]. The seed synthesis is a REDOX reaction. For that, $HAuCl_4 \cdot 3H_2O$ gold salt is used, and the reducing agent is citrate. Given that the standard reduction potentials don't favour thermodynamically the reaction between these two compounds, the reduction was carried out at boiling temperature. The adsorption of the citrate and 1,3-acetone dicarboxylate molecules on the NPs surface confers electrostatic stability [23] because it favours considerably the repulsions between them, giving the surface of the NPs a negative charge. Then, the seeds were grown [22] with Ag via chemical reduction of a silver salt, obtaining Au@Ag NPs of ca. d=30nm after a first growth, and ca. d=50nm after a second growth. This is also a REDOX reaction. AgNO3 silver salt is used, and the reducing agent is the Fe-citrate complex. The complexation of Fe (II) with citrate diminishes the Fe^{3+}/Fe^{2+} standard reduction potential, so in this stage the reaction is thermodynamically favourable and can be carried out at room temperature [22].

Given the fact that we couldn't characterize the NPs via TEM, we cannot know their exact dimensions. Consulting the literature [22], we can know that the method described above will result in the indicated NP sizes.

All NPs were characterized via UV-visible spectrophotometry during the process [Figure 10].

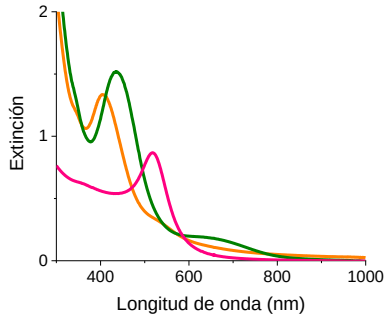

Figure 10. UV-vis spectra for the 14 nm Au NPs (pink), 30 nm Au@Ag NPs (orange) and 50 nm Au@Ag (green).

In the spectra [Figure 10] we can observe that the LSPR band for the 14nm Au NPs (seeds) happens at λ = 517 nm, according to the dielectric properties of Au [5]. When the NPs are coated by a first Ag layer (30 nm Au@Ag NPs), the LSPR shifts to lower wavelengths: λ = 404 nm. Although the particles grow in size, the wavelength decreases due to the dielectric properties of Ag, different to those of Au. As the NPs are coated by a second Ag layer (50 nm Au@Ag NPs), the deposition of Ag atoms on the NPs surface shifts the LSPR band to higher wavelengths: λ = 404 nm, due to the increase in size. The observed band around 680 nm on the 50 nm Au@Ag NPs [Figure 10] indicates a polydisperse solution, with presence of NPs of other sizes and shapes.

5.2. Formation and characterization of Au nanocapsules

Au@Au core-shell nanocapsules are formed (Au nanocapsules) using the 50nm Au@Ag NPs as templates. In this case, it is necessary to add a new stabilizing agent in the medium, since the electrostatic stabilization from the citrate is not enough to allow the formation of nanocapsules. For that, CTAB is added, a long-chain molecule that binds to the NPs via physisorption through the bromures, forming a bilayer [24], after an exchange reaction with the citrate. CTAB addition confers a great steric and electrostatic stability [23] through the quaternary amines, which provide positive charge to the NP surfaces. After the Au@Ag NPs have been functionalized with CTAB, we proceed to the formation of Au nanocapsules via galvanic replacement, combined with the correduction using a mild reducing agent. These are REDOX reactions. The galvanic replacement is based on the oxidation of the metal that conforms the exterior coating of the NPs, and the reduction of a metal that is added in the form of a salt. The gold salt used is $HAuCl_4 \cdot 3H_2O$. According to this, the Ag on the exterior part of the NPs is oxidized, donating electrons and reducing the Au (III) of the added salt in Au (0) [reaction 1]. The Au (0) is then deposited on the surface of the Ag NPs. The correduction is based on the reduction of one of more metals that are in an oxidation state superior to 0 (i.e. they are dissolved), by a reducing agent that is added to the system. The mild reducing agent used is AA, which reduces the Au (III) to Au (0) [reaction 2] and the Ag (I) to Ag (0) [reaction 3]. The standard reduction potentials [22,25] are thermodynamically favourable for all the possible reactions, thus they are all developed at room temperature.

$3 \times (Ag \rightarrow Ag^+ + 1\ e^-)$ Ox. de Ag (0) a Ag (I) $E°$= - 0.80 V

$\underline{AuCl_4^- + 3\ e^- \rightarrow Au + 4Cl^-}$ Red. de Au (III) a Au (0) $E°$= + 1.52 V

$3\ Ag + AuCl_4^- \rightarrow 3\ Ag^+ + Au + 4\ Cl^-$ $E°$= + 0,72 V

$3\ Ag\ (s) + HAuCl_4\ (aq) \rightarrow 3\ AgCl\ (aq) + Au\ (s) + HCl\ (aq)$ [1]

$3 \times (C_6H_7O_6^- \rightarrow C_6H_5O_6^- + 2\ H^+ + 2\ e^-)$ Ox. de ascorbato a dehidroascorbato $E°$= -0.35 V

$\underline{2 \times (AuCl_4^- + 3\ e^- \rightarrow Au + 4Cl^-)}$ Red. de Au (III) a Au (0) $E°$= + 1.52 V

$3\ C_6H_7O_6^- + 2\ AuCl_4^- \rightarrow 3\ C_6H_5O_6^- + 6\ H^+ + 2\ Au + 8\ Cl^-$ $E°$= + 1.17 V

$3\ C_6H_8O_6\ (aq) + 2\ HAuCl_4\ (aq) \rightarrow 3\ C_6H_6O_6\ (aq) + 8\ HCl\ (aq) + 2\ Au\ (s)$ [2]

$C_6H_7O_6^- \rightarrow C_6H_5O_6^- + 2\ H^+ + 2\ e^-$ Ox. de ascorbato a dehidroascorbato $E°$= -0.35 V

$\underline{2 \times (Ag^+ + 1\ e^- \rightarrow Ag)}$ Red. de Ag (I) a Au (0) $E°$= + 0.80 V

$C_6H_7O_6^- + 2\ Ag^+ \rightarrow C_6H_5O_6^- + 2\ H^+ + 2\ Ag$ $E°$= + 0.45 V

$C_6H_8O_6\ (aq) + 2\ AgCl\ (aq) \rightarrow C_6H_6O_6\ (aq) + 2\ HCl\ (aq) + 2\ Ag\ (s)$ [3]

The spectra observed during the formation of the Au nanocapsules are depicted in [Figure 11].

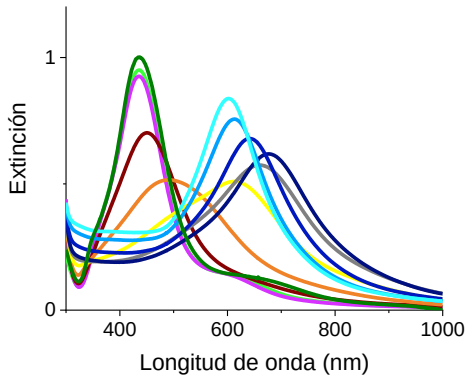

Figure 11. UV-visible spectra for the galvanic replacement process resulting in Au nanocapsules: 50 nm Au@Ag NPs (dark green), + CTAB (light green), + AA (lilac), + 250 µL $HAuCl_4$ (brown), + 500 µL $HAuCl_4$ (orange), + 750 µL $HAuCl_4$ (yellow), + 1 mL $HAuCl_4$ (grey), + 1.250 mL $HAuCl_4$ (navy blue), + 2 mL $HAuCl_4$ (dark blue), + 3 mL $HAuCl_4$ (light blue), + 4 mL $HAuCl_4$ (cerulean).

In the spectra [Figure 11], it is observed that small additions of $HAuCl_4$ cause the LSPR to shift to higher wavelengths and a global intensity decrease. This may be due the loss of Ag, suggesting that the reactive process is governed by the galvanic replacement reaction [reaction 1]. For every Au (III) reduced to Au (0), three Ag atoms are oxidized. After the addition of approximately 1 mL of $HAuCl_4$, the LSPR starts shifting back to lower wavelengths and higher intensities. Here, the spectral shift as a function of the amount of Au salt is more progressive, in comparison to the beginning of the process. This may be due to the deposition of Au atoms on the NPs surface, suggesting that the reactive process is now governed by the correduction reaction of the Au (III) [reaction 2]. In it, Au (III) is reduced to Au (0), while no Ag atom gets oxidized.

Given that the process of the formation of Au nanocapsules could only be characterized via UV-vis spectroscopy [Figure 11], it becomes necessary to consult the literature to better understand the process. Polavarapu et al. [12] carried out the formation of Au nanocapsules (reactive conditions were analogous to the ones just described). They used Au@Ag core-shell NPs with prism morphology as templates for the galvanic replacement, combined with correduction using AA, and characterized the process by UV-vis spectroscopy, TEM and X-ray computed tomography. At the beginning of the process, they observed superficial erosion predominantly on the vertices and edges, and the posterior deposition of Au atoms in those spaces. Next, a thin layer of Au-Ag alloy covered practically all the surface, giving place to the first cavities. By increasing the amount of gold salt, the Ag-Au alloy shell began to be clearly visualized, simultaneously to the enlargement of the cavities, to the point in which a thin Au layer covered the Ag-Au alloy shell. Following further addition of the gold salt, the further growth of the shell was only based on Au atoms. As the particles grew further, their original morphology progressively turned into the final octahedral shape. Thus, Polavarapu et al., distinghished clearly two stages in the process of formation of the nanocapsules: a first stage, governed by the galvanic replacement reaction [reaction 1], where the Ag-Au capsule is formed while the Ag (I) to Ag (0) correduction by the AA [reaction 3] confers certain control over the process, attenuating the stoichiometric difference between the Au and Ag atoms in the galvanic replacement. And a second stage, governed by the correduction of the Au (III) to Au (0) by the AA [reaction 2], where the capsule increased its shape via deposition of Au atoms. Results obtained led them to establish a 40:60 ratio of Ag-Au alloy as the turning point that separates the first from the second stage.

Now it is possible to understand better the UV-vis spectra that we obtained during the Au nanoparticle formation [Figure 11]. The first stage begins with the addition of $HAuCl_4$ and finishes when ca. 1 mL has been added. The reactions that govern this stage are the galvanic replacement [reaction 1] and the correduction by AA of the oxidized Ag [reaction 3] during galvanic replacement. The LSPR band shifts to higher wavelengths, and intensity decreases due to the formation of cavities and the loss of Ag atoms in the NPs. The stoichiometry of the corresponding reactions provides us with an explanation to the observed progression in the LSPR shifts. The second stage begins upon the addition of 1 mL of $HAuCl_4$ approx. The reaction that governs this stage is the correduction of the Au (III) from the salt, by the AA [reaction 2]. The LSPR band shifts slightly to lower wavelengths and intensity increases, due to the thickening of the shell [13,14] by the deposition of Au atoms on the NPs surface. Again, the stoichiometry of the corresponding reaction explains the progression of the LSPR shift.

5.3. Formation and characterization of Pd nanocapsules

At this moment, the synthesis of nanocapsules composed entirely by Pd, of which plasmonic and catalytic properties can be taking in advantage, is an objective to reach by a large number of investigation groups, and it was also the objective of this thesis. The thermic stability of the Pd makes it a better candidate for working under certain conditions. Due to the impossibility to experiment in the laboratory with NPs formed entirely by Pd because of the COVID-19 pandemic, and the shortage of literature on the matter, it has been decided to shift the focus to nanocapsules formed by Pd alloyed with Ag and/or Au, in which plasmonic properties are provided by Ag and/or Au, and the catalytic properties are provided by Pd. An example is the work of Jing et al., who synthesized Ag-Pd nanocapsules using Ag nanocubes as templates. They use two different procedures: galvanic replacement combined with correduction by a mild reducing agent (same way as in the formation of Au nanocapsules covered in this work), and galvanic replacement without the combination with correduction. All are REDOX reactions. For the galvanic replacement they used the palladium salt H_2PdCl_4. In this context, the Ag that conforms the exterior part of the NPs is oxidized, donating electrons and reducing the Pd (II) of the added salt to Pd (0) [reaction 4]. The Pd (0) is deposited on the surface of the Ag NPs. In their setup, the correduction is based on the reduction of one of more metals that are in an oxidation state superior to 0 (i.e. they are dissolved). In this context, the AA added reduces the Pd (II) to Pd (0) [reaction 5] and the Ag (I) to Ag (0) [reaction 6]. The standard reduction potentials [22,25,26] to the galvanic replacement are not thermodynamic favourable; hence, a temperature of 100°C is required [26].

$2\ x\ (Ag \rightarrow Ag^+ + 1\ e^-)$	Ox. de Ag (0) a Ag (I)	$E°$= - 0.80 V	
$PdCl_4^{2-} + 2\ e^- \rightarrow Pd + 4Cl^-$	Red. de Pd (II) a Pd (0)	$E°$= + 0.591 V	
$2\ Ag + PdCl_4^{2-} \rightarrow 2\ Ag^+ + Pd + 4\ Cl^-$		$E°$= - 0.209 V	[4]
$2\ Ag\ (s) + H_2PdCl_4\ (aq) \rightarrow 2\ AgCl\ (aq) + Pd\ (s) + 2\ HCl\ (aq)$			

$C_6H_7O_6^- \rightarrow C_6H_5O_6^- + 2\ H^+ + 2\ e^-$	Ox. de ascorbato a dehidroascorbato	$E°$= -0.35 V	
$PdCl_4^{2-} + 2\ e^- \rightarrow Pd + 4Cl^-$	Red. de Pd (II) a Pd (0)	$E°$= + 0.591 V	
$C_6H_7O_6^- + PdCl_4^{2-} \rightarrow C_6H_5O_6^- + 2\ H^+ + Pd + 4Cl^-$		$E°$= + 0.241 V	[5]
$C_6H_8O_6\ (aq) + H_2PdCl_4\ (aq) \rightarrow C_6H_6O_6\ (aq) + 4\ HCl\ (aq) + Pd\ (s)$			

$C_6H_7O_6^- \rightarrow C_6H_5O_6^- + 2\ H^+ + 2\ e^-$	Ox. de ascorbato a dehidroascorbato	$E°$= -0.35 V	
$2\ x\ (Ag^+ + 1\ e^- \rightarrow Ag)$	Red. de Ag (I) a Au (0)	$E°$= + 0.80 V	
$C_6H_7O_6^- + 2\ Ag^+ \rightarrow C_6H_5O_6^- + 2\ H^+ + 2\ Ag$		$E°$= + 0.45 V	[6]
$C_6H_8O_6\ (aq) + 2\ AgCl\ (aq) \rightarrow C_6H_6O_6\ (aq) + 2\ HCl\ (aq) + 2\ Ag\ (s)$			

First, we will comment the UV-vis spectra they obtained [Figure 12] [26] upon formation of Ag-Pd nanocapsules via galvanic replacement combined with the correduction by AA (same procedure as in this work for the formation of Au nanocapsules [figure 11]). Also, TEM images of the formative process are included [figure 13] [26], which make it easier to follow.

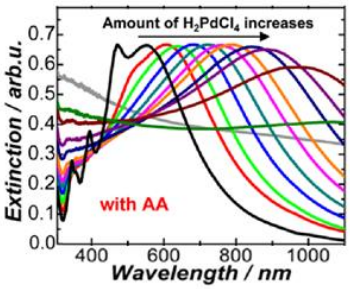

Figure 12. UV-visible spectra for the galvanic replacement process using Pd over Ag nanocubes, under the presence of AA [26]*. [Consult reference for more information].

In the spectra [Figure 12] we can observe that the addition of H_2PdCl_4 makes the LSPR shift to higher wavelengths, encompassing almost totally the visible and near-IR spectrum and maintaining a practically constant intensity. This is because the Ag atoms are causing the LSPR band [26], and it is possible due to two reasons: 1) the stoichiometry of the galvanic replacement reaction [reaction 4], by which for every Pd (II) reduced to Pd(0), two Ag atoms are oxidized. This stoichiometry confers a certain control of the situation, assisted by the reduction of the Ag oxidized by the AA [reaction 6]; 2) the required temperature for the galvanic replacement favours kinetically the interdiffusion of the Pd atoms through the Ag matrix, so that the Ag atoms position on the surface and become responsible for the majority of the plasmonic response in the NPs. A point is reached when the LSPR band begins to diminish its intensity, paired to the progressive loss of the dipolar plasmon. This can be explained by the presence of Pd atoms on the surface, which makes them cause the LSPR bands. Thus, analogously to the already covered process for Au nanocapsules (see **5.2.**), the formation of Pd nanocapsules is developed through the same two stages: a first stage, governed by the galvanic replacement reaction [reaction 4], where the Ag-Pd capsule is formed while the Ag (I) to Ag (0) correduction by the AA [reaction 6] confers certain control over the process, attenuating the stoichiometric difference between the Pd and Ag atoms in the galvanic replacement. And a second stage, governed by the correduction of the Pd (II) to Pd (0) by the AA [reaction 5], in which

the Ag-Au capsule increases its shape due solely to the deposition of Pd atoms. Chen et al. determined that the inflexion point between the two stages is produced when a molar relation between 33% and 49% for the Pd is achieved.

The AA has a fundamental role from the very beginning of the process, because the initial corrosion of the Ag produced in different NPs zones [Figure 13] opens the way to multitude of porosities and, consequently, to the formation of a more extense alloy surface. This amplification of the reacting surface is also favoured by the easy interdiffusion of the Ag and Pd atoms within the alloy matrix. Given that the reactions photocatalyzed by Pd take place on the NPs surface, achieving a higher area means a higher reacting yield.

Figure 13. TEM images for the galvanic replacement process using Pd over Ag nanocubes, under the presence of AA [26]*. [Consult reference for more information].

We will now briefly discuss the the UV-vis spectra [Figure 14] [26] obtained by Jing. Et al. for the same process of Ag-Pd nanocapsule synthesis as before, but without using a mild reducing agent.

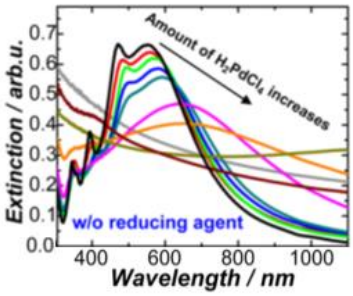

Figure 14. UV-visible spectra for the galvanic replacement process using Pd over Ag nanocubes, without the presence of AA [26]*. [Consult reference for more information].

In the spectra [Figure 14] we can observe that the addition of H_2PdCl_4 makes the LSPR shift to higher wavelengths, but the LSPR peaks dampen out after a brief shift along the visible spectrum, until the dipolar plasmon is lost. Due to the lack of a mild reducing agent, the Ag that oxidizes during galvanic replacement [reaction 4] does not get reduced [reaction 6], and the molar relation Ag:Pd, which stops the alloying process, is achieved much sooner. Hence, the Pd causes the observed LSPR band. TEM images [Figure 15] [26] show initial corrosion in the nanocubes' corners, which removes the ability to generate cavities in a disperse and distributed way (like the ones observed using AA [Figure 13]) that would lead to the amplification of the reacting surface and also speed up the loss of the dipole plasmon resonance.

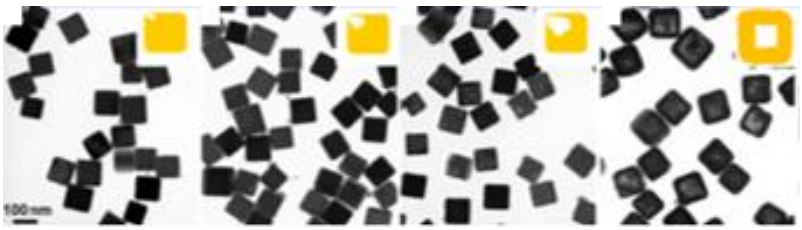

Figure 15. TEM images for the galvanic replacement process using Pd over Ag nanocubes, without the presence of AA [26]*. [Consult reference for more information].

5.4. Analysis of the catalytic capacities of Pd nanocapsules

As already mentioned, the formation of Pd capsules with advantageous plasmonic and catalityc properties is currently in developement. On the other hand, a lot of research has already covered the catalytic capacitation of nanocapsules with Pd alloyed with Ag and/or Au. The Pd provides catalytic capacities, while the Ag and Au provide their plasmonic properties. For example, Jing et al., Sarina et al. and Cobley et al. carried out experiments that demonstrate that Ag-Pd and Au-Pd alloys conform a great tandem when used as reacting surfaces in catalytic processes [17,26,27]. Cobley et al. studied the variation of the rate constant k for the hydrogenation of the methyl red indicator on Ag-Pd and Ag-Pd-Au surfaces. The results obtained not only make evident the efficiency of the Pd as catalyst in this type of reactions; for Ag-Pd-Au trimetallic alloys they also underline the importance in the addition order of the Pd and Au salts in the galvanic replacement process. The composition of the synthesized nanocapsules via galvanic replacement without correduction, specifying the order of addition of the Pd and Au salts for their formation, as well as the rate constant obtained, are collected in Table 2.

Table 2. Alloy ratios of the nanocapsules, with the rate constants obtained. The concentrations of the Pd and Au salts were the same in each addition, except in experiment (iv) [consult reference for more information].

Order of addition in galvanic replacement	Ag-Au-Pd alloy ratios in shells (%)	k / mol Pd (s^{-1})
Ag NPs + Pd (II) salt	79:0:21	3.5×10^7
Ag NPs + Au (I) salt + Pd (II) salt	63:20:17	2.3×10^7
Ag NPs + Pd (II) salt + Au (I) salt	55:17:28	3.1×10^7
Ag NPs + Pd (II) salt + (2x) Au (I) salt	21:64:25	0.4×10^7

The Ag-Pd nanocapsules [Table 2 (i)] combine the capacity of absorption of the Ag and the catalytic power of the Pd. If the galvanic replacement is continued on these Ag-Pd nanocapsules by adding the gold salt [Table 2 (iii)], a trimetallic alloy is formed. In the last moments of the galvanic replacement, a process of dealloying or excessive transmetalation initiates. This causes great porosity on the nanocapsules, and can fragment them if not stopped in time [Table 2(iv)]. However, when forming trimetal Ag-Pd-Au nanocapsules, if the Au salt is added prior to the Pd salt [Table 2 (ii)], nanocapsules with much less porosity are obtained [17]. This is due to the fact that the Ag-Pd alloy does not suffer an excessive transmetalation. Instead, the galvanic replacement process stops before this happens, and adding any excess of Pd salt won't cause fragmentation.

Another study about the catalytic capacities of Ag-Pd nanocapsules, this time focused on an application at an industrial level, was carried out by Liu et al. [28] Reducing the emission of toxic and greenhouse gases has become a major goal when chemistry procedures are designed. The usage of H_2 (g) instead of fossil fuels as an energy source is being widely considered, so new mechanisms of obtention are currently being researched. Liu et al. studied the obtention of H_2 (g) from formaldehyde, a toxic compound, secondary product of the biomass gasification process that is utilized in multitude of procedures in the industry. They used Ag-Pd nanocapsules with different alloy ratios as catalysts, under electromagnetic radiation in the visible zone. The highest

catalytic capacity is achieved when both metals have a presence of 50% in the alloy. Higher Pd proportions show a lower reacting yield.

6. Conclusions

Using the synthesis of Au nanocapsules as a model system, this work verifies that galvanic replacement combined with correduction is an efficient technique, by which it is possible to obtain structures with outstanding plasmonic responses in the UV-vis and near-IR ranges. The plasmonic responses of the NPs can strengthen properties that are inherent to the materials themselves. This way, Pd nanocapsules with an efficient plasmonic response could greatly enhance the catalytic properties inherent to the material, and lead to Pd NPs that are highly efficient for photocatalysis. Due to the impossibility to do experiments on the formation of Pd nanocapsules caused by the COVID-19 pandemic, the corresponding part on the formation of Pd nanocapsules of this thesis has been replaced with a bibliographic revision that covers the synthesis and photocatalytic properties of Ag-Pd nanocapsules. The reviewed literature shows that the synthesis of these Ag-Pd nanocapsules through galvanic replacement combined with the correduction by a mild reducing agent is an effective formative process: the nanocapsules' morphology full of pores and cavities increases the reactive surface, and the Ag plasmonic response notably increases the catalytic capacity of the Pd. Existing research avails that the use of Ag-Pd nanocapsules as reacting surfaces in reactions catalysed by Pd translates in an increase of the yield and productivity achieved. For this reason, the incorporation of Ag-Pd nanocapsules consolidates as a very promising technology for the optimization of a myriad of processes from small-scale reactions up to industrial scale.

7. Bibliography

(1) Liz Marzán, L.; Guerrero Martínez, A.; Alvarez Puebla, R. Nanoplasmónica Basada En Química Coloidal. *An. la Real Soc. Española Química* **2011**, *107* (3), 221–228.

(2) García, M. A. Plasmones de superficie en nanopartículas metálicas. ¿Qué son y para qué sirven? https://www.youtube.com/watch?v=LK7hlYPvmIQ (accessed May 1, 2020).

(3) Mayer, K. M.; Hafner, J. H. Localized Surface Plasmon Resonance Sensors. *Chem. Rev.* **2011**, *111* (6), 3828–3857. https://doi.org/10.1021/cr100313v.

(4) Garcia, M. A. Surface Plasmons in Metallic Nanoparticles: Fundamentals and Applications. *J. Phys. D. Appl. Phys.* **2012**, *45* (38). https://doi.org/10.1088/0022-3727/45/38/389501.

(5) Yu, R.; Liz-Marzán, L. M.; García De Abajo, F. J. Universal Analytical Modeling of Plasmonic Nanoparticles. *Chem. Soc. Rev.* **2017**, *46* (22), 6710–6724. https://doi.org/10.1039/c6cs00919k.

(6) Khlebtsov, N. G.; Dykman, L. A. Optical Properties and Biomedical Applications of Plasmonic Nanoparticles. *J. Quant. Spectrosc. Radiat. Transf.* **2010**, *111* (1), 1–35. https://doi.org/10.1016/j.jqsrt.2009.07.012.

(7) Xia, Y.; Campbell, D. J. Plasmons: Why Should We Care? *J. Chem. Educ.* **2007**, *84* (1), 91. https://doi.org/10.1021/ed084p91.

(8) De Abajo, F. J. G. Nonlocal Effects in the Plasmons of Strongly Interacting Nanoparticles, Dimers, and Waveguides. *J. Phys. Chem. C* **2008**, *112* (46), 17983–17987. https://doi.org/10.1021/jp807345h.

(9) Chen, J.; Wiley, B.; McLellan, J.; Xiong, Y.; Li, Z. Y.; Xia, Y. Optical Properties of Pd-Ag and Pt-Ag Nanoboxes Synthesized via Galvanic Replacement Reactions. *Nano Lett.* **2005**, *5* (10), 2058–2062. https://doi.org/10.1021/nl051652u.

(10) Genç, A.; Patarroyo, J.; Sancho-Parramon, J.; Bastús, N. G.; Puntes, V.; Arbiol, J. Hollow Metal Nanostructures for Enhanced Plasmonics: Synthesis, Local Plasmonic Properties and Applications. *Nanophotonics* **2017**, *6*

(1), 193–213. https://doi.org/10.1515/nanoph-2016-0124.
(11) Xia, X.; Wang, Y.; Ruditskiy, A.; Xia, Y. 25th Anniversary Article: Galvanic Replacement: A Simple and Versatile Route to Hollow Nanostructures with Tunable and Well-Controlled Properties. *Adv. Mater.* **2013**, *25* (44), 6313–6333. https://doi.org/10.1002/adma.201302820.
(12) Polavarapu, L.; Zanaga, D.; Altantzis, T.; Rodal-Cedeira, S.; Pastoriza-Santos, I.; Pérez-Juste, J.; Bals, S.; Liz-Marzán, L. M. Galvanic Replacement Coupled to Seeded Growth as a Route for Shape-Controlled Synthesis of Plasmonic Nanorattles. *J. Am. Chem. Soc.* **2016**, *138* (36), 11453–11456. https://doi.org/10.1021/jacs.6b06706.
(13) Gao, Z.; Ye, H.; Wang, Q.; Kim, M. J.; Tang, D.; Xi, Z.; Wei, Z.; Shao, S.; Xia, X. Template Regeneration in Galvanic Replacement: A Route to Highly Diverse Hollow Nanostructures. *ACS Nano* **2020**, *14* (1), 791–801. https://doi.org/10.1021/acsnano.9b07781.
(14) Prodan, E.; Radloff, C.; Halas, N. J.; Nordlander, P. A Hybridization Model for the Plasmon Response of Complex Nanostructures. *Science (80-.).* **2003**, *302* (5644), 419–422. https://doi.org/10.1126/science.1089171.
(15) Sperling, R. A.; Parak, W. J. Surface Modification, Functionalization and Bioconjugation of Colloidal Inorganic Nanoparticles. *Philos. Trans. R. Soc. A Math. Phys. Eng. Sci.* **2010**, *368* (1915), 1333–1383. https://doi.org/10.1098/rsta.2009.0273.
(16) Schwartzberg, A. M.; Oshiro, T. Y.; Zhang, J. Z.; Huser, T.; Talley, C. E. Improving Nanoprobes Using Surface-Enhanced Raman Scattering from 30-Nm Hollow Gold Particles. *Anal. Chem.* **2006**, *78* (13), 4732–4736. https://doi.org/10.1021/ac060220g.
(17) Cobley, C. M.; Campbell, D. J.; Xia, Y. Tailoring the Optical and Catalytic Properties of Gold-Silver Nanoboxes and Nanocages by Introducing Palladium. *Adv. Mater.* **2008**, *20* (4), 748–752. https://doi.org/10.1002/adma.200702501.
(18) Xiao, M.; Jiang, R.; Wang, F.; Fang, C.; Wang, J.; Yu, J. C. Plasmon-Enhanced Chemical Reactions. *J. Mater. Chem. A* **2013**, *1* (19), 5790–5805. https://doi.org/10.1039/c3ta01450a.
(19) Universitat Politècnica de València. Microscopía electrónica de transmisión http://www.upv.es/entidades/SME/info/753329normalc.html (accessed May 1, 2020).
(20) Stetefeld, J.; McKenna, S. A.; Patel, T. R. Dynamic Light Scattering: A Practical Guide and Applications in Biomedical Sciences. *Biophys. Rev.* **2016**, *8* (4), 409–427. https://doi.org/10.1007/s12551-016-0218-6.
(21) Schulz, F.; Homolka, T.; Bastús, N. G.; Puntes, V.; Weller, H.; Vossmeyer, T. Little Adjustments Significantly Improve the Turkevich Synthesis of Gold Nanoparticles. *Langmuir* **2014**, *30* (35), 10779–10784. https://doi.org/10.1021/la503209b.
(22) Carbó, E.; Fernández, C.; Fernández, J.; Pastoriza, I.; Pérez, J. The Versatility of Fe (II) in the Synthesis of Uniform Citrate Stabilized Plasmonic Nanoparticles with Tunable Size at Room Temperatura. *Univ. Vigo.* **2020**.
(23) Gómez, F. Síntesis de Complejos y Estabilización de Nanopartículas de Paladio Con Ligandos Híbridos Pirazólicos y Carbenos N-Heterocíclicos y Su Aplicación En Catálisis. *Tesis Dr. Dep. Química. Fac. Ciencias. Univ. Autònoma Barcelona.* **2013**.
(24) Li, R.; Wang, Z.; Gu, X.; Chen, C.; Zhang, Y.; Hu, D. Study on the Assembly Structure Variation of Cetyltrimethylammonium Bromide on the Surface of Gold Nanoparticles. *ACS Omega* **2020**, *5* (10), 4943–4952. https://doi.org/10.1021/acsomega.9b03823.
(25) Matsui, T.; Kitagawa, Y.; Okumura, M.; Shigeta, Y. Accurate Standard Hydrogen Electrode Potential and Applications to the Redox Potentials of Vitamin C and NAD/NADH. *J. Phys. Chem. A* **2015**, *119* (2), 369–376. https://doi.org/10.1021/jp508308y.
(26) Jing, H.; Wang, H. Structural Evolution of Ag−Pd Bimetallic Nanoparticles through Controlled Galvanic Replacement: Effects of Mild Reducing Agents. **2015**. https://doi.org/10.1021/acs.chemmater.5b00199.
(27) Sarina, S.; Zhu, H.; Jaatinen, E.; Xiao, Q.; Liu, H.; Jia, J.; Chen, C.; Zhao, J. Enhancing Catalytic Performance of Palladium in Gold and Palladium Alloy Nanoparticles for Organic Synthesis Reactions through Visible Light Irradiation at Ambient Temperatures. *J. Am. Chem. Soc.* **2013**, *135* (15), 5793–5801. https://doi.org/10.1021/ja400527a.
(28) Liu, H.; Wang, M.; Zhang, X.; Ma, J.; Lu, G. High Efficient Photocatalytic Hydrogen Evolution from Formaldehyde over Sensitized Ag@Ag-Pd Alloy Catalyst under Visible Light Irradiation. *Appl. Catal. B Environ.* **2018**, *237* (April), 563–573. https://doi.org/10.1016/j.apcatb.2018.06.028.